JOURNAL OF GEOPHYSICAL RESEARCH, VOL. 115, B02205, doi:10.1029/2009JB006422, 2010

Lithospheric thinning and localization of deformation during Rayleigh-Taylor instability with nonlinear rheology and implications for intracontinental magmatism

Christopher Harig,[1] Peter Molnar,[1] and Gregory A. Houseman[2]

Received 2 March 2009; revised 4 August 2009; accepted 30 September 2009; published 17 February 2010.

[1] Thinning of mantle lithosphere due to Rayleigh-Taylor instability can be a mechanism for triggering continental magmatism near active or recently active plate boundaries. We consider whether it is also plausible as a mechanism for intracontinental magmatism, several hundred kilometers from active subduction or rifting. We perform two-dimensional Rayleigh-Taylor experiments and find that a shear stress-free top and non-Newtonian flow permit two types of instability to develop, largely dependent on how the viscosity coefficient varies with depth. For small variation with depth, with the *e*-folding depth scale (the interval across which the coefficient changes by a factor of *e*) greater than a third to a half of the thickness of the unstable layer, deformation concentrates at the ends of the layer in localized thinning and thickening zones; the middle part moves horizontally toward the region of thickening as a coherent block undergoing minimal strain. When the viscosity coefficient decreases more rapidly with depth, thinning of the layer is distributed laterally over a wide zone. Between the regions of thickening and thinning, shear strain and vertical gradients in horizontal velocity prevent this area from moving as a coherent block. The rheological exponent, n, that relates strain rate to stress in the constitutive equation controls the degree of localization of the downwelling and upwelling: the width varies as $\approx n^{-1/2}$. In intraplate settings where a shear stress-free top condition could be applicable, high-stress crystalline plasticity could provide a mechanism for the narrow zones of thinning and upwelling, which would facilitate decompression related volcanism.

Citation: Harig, C., P. Molnar, and G. A. Houseman (2010), Lithospheric thinning and localization of deformation during Rayleigh-Taylor instability with nonlinear rheology and implications for intracontinental magmatism, *J. Geophys. Res.*, *115*, B02205, doi:10.1029/2009JB006422.

1. Introduction

[2] Continental magmatism is a common occurrence in tectonically active regions of subduction or rifting. Subduction zone arc magmatism is produced mainly through chemical interaction between the subducted crust and mantle material [e.g., *Kay*, 1980; *Morris et al.*, 1990]. Rifting, on the other hand, thins lithosphere to allow the underlying asthenosphere to melt through adiabatic decompression as it rises [e.g., *McKenzie and Bickle*, 1988]. How then do we explain continental magmatism, that occurs several hundred kilometers from plate boundaries (e.g., northern Tibetan plateau, the North China Craton), in the absence of these tectonic processes? Barring heat sources from below, produced perhaps by mantle plumes, or the introduction of a chemical process, we are left to explore another way to thin lithosphere and generate melt [e.g., *Elkins-Tanton*, 2005].

[3] Dynamic, ductile removal of lower lithosphere is one possibility that creates the accommodation space required for the rise of material and hence either decompression melting or melting from conductive heating of shallower lithosphere. With plausible conditions, the Rayleigh-Taylor instability of the mantle lithosphere when perturbed enough can thin the lithosphere to a significant degree (by tens of percent) to overcome stabilization by thermal diffusion [e.g., *Conrad and Molnar*, 1997; *Gemmer and Houseman*, 2007; *Hoogenboom and Houseman*, 2006; *Molnar et al.*, 1998; *Molnar and Houseman*, 2004]. Additionally, if part of the crust has been transformed into eclogite, its density [e.g., *Jull and Keleman*, 2001; *Kay and Kay*, 1993] and low viscosity [*Austrheim*, 1991] allow it to participate in the downwelling/removal of mantle lithosphere [e.g., *Farmer et al.*, 2002]. The inclusion of eclogite in a Rayleigh-Taylor process would also contribute to the effective thickness of the unstable layer, which affects the lateral extent of eventual thinning. For instance, the Sierra Nevada shows evidence of removal of a 40–60 km thick eclogitic layer in addition to the underlying mantle lithosphere [*Ducea and Saleeby*, 1996]. *Jull and Keleman* [2001] found a variety of lower crustal compositions that can develop instabilities in layers only 10 km thick on relevant timescales.

[1] Department of Geological Sciences, Cooperative Institute for Research in Environmental Science, University of Colorado at Boulder, Boulder, Colorado, USA.
[2] Institute of Geophysics and Tectonics, School of Earth and Environment, University of Leeds, Leeds, UK.

0148-0227/10/2009JB006422$09.00

[4] With Rayleigh-Taylor instabilities, removed lower lithosphere is replaced with less dense asthenosphere, and the effects of this process are seen with a variety of observations. Geomorphic observations such as regional surface uplift and/or tilting [e.g., *Stock et al.*, 2004; *Unruh*, 1991], seismic observations including low seismic wave speeds [e.g., *Jones et al.*, 1994; *Reeg et al.*, 2007], and geochemically, the appearance of high-potassium magmas can all result from thinned lithosphere [*Farmer et al.*, 2002; *Hoernle et al.*, 2006; *Kay and Kay*, 1993; *Turner et al.*, 1996]. Perhaps because of the difficulty of inferring the previous state of the lithosphere through time, these instabilities commonly have been suggested to apply to regions of recent tectonic activity (<10 Myr) such as the Sierra Nevada in California [e.g., *Ducea and Saleeby*, 1996; *Lee et al.*, 2001; *Jones et al.*, 2004], sections of the Andes [e.g., *Kay and Kay*, 1993], New Zealand [e.g., *Stern et al.*, 2000, 2006], and the southeast Carpathians in the Vrancea region [e.g., *Knapp et al.*, 2005].

[5] In each of these locations, the inferred downwelling zone must be compensated by an adjacent zone of lithospheric thinning; for instance the Vrancea downwelling is accompanied by thinning of the mantle lithosphere beneath the Transylvanian basin [*Lorinczi and Houseman*, 2009]. Often, in the absence of evidence indicating the location of downwelling flow, removed lithosphere is assumed to have sunk immediately below regions of thin lithosphere. Another characteristic of these regions of thin lithosphere is that they share a regional length scale. The lateral extent of such regions often covers at least 100 km, sufficient for resolution by key observation techniques such as travel time tomography, where densely spaced seismic networks have been deployed [e.g., *Reeg et al.*, 2007].

[6] In many regions that have been affected by previous, subducted slab-related metasomatism, removal of mantle lithosphere has been accompanied by potassic magmatism. Although it is possible for magma to be generated from the sinking of detached, downwelling mantle lithosphere [*Elkins-Tanton*, 2005, 2007], high-potassium instability-generated melts have been more commonly ascribed to thinning of lithosphere [*Elkins-Tanton and Grove*, 2003; *Farmer et al.*, 2002; *Hoernle et al.*, 2006; *Kay and Kay*, 1993; *Lee et al.*, 2001; *Manley et al.*, 2000; *Turner et al.*, 1996]. Not all continental potassic magmatism is related to lithosphere instabilities, however [e.g., *Farmer et al.*, 2008], and it is unknown whether potassium and hydroxyl-rich (water rich) zones in the mantle can contribute to conditions needed for lithospheric removal. Still, at present the localization of high-potassium magmas seems the best indicator for lithospheric instabilities that occur on short length scales, or for those that occurred sufficiently far into the past that other indicators may have been lost. Building on earlier work, we investigate how this signature magmatism could be related to the localized thinning of the lithosphere.

[7] *Houseman and Molnar* [1997] found, using numerical experiments of Rayleigh-Taylor instability of a layer with stress-dependent viscosity and a rigid upper surface, that for long perturbation wavelengths, deformation was more localized above upwelling/downwellings than for shorter wavelengths or for cases with Newtonian viscosity. In general the wavelength of maximum growth rate is about three times the unstable layer thickness. Thus it would seem that lithospheric thinning need not occur immediately adjacent to downwelling but could be displaced a distance several times the thickness of the unstable layer. When wavelength is increased for a shear stress-free upper boundary, the wide separation of the upwelling zone from the downwelling implies that thinning of lithosphere, and related magmatism, could occur in narrow groupings hundred of kilometers from the downwelling perhaps in the absence of upper crustal deformation. In some cases, this could be several hundred kilometers from previous zones of subduction and might be described as intraplate volcanism.

[8] In several continental regions with potassic magmatism hundreds of kilometers from plate boundaries, the link to a tectonic or dynamic mechanism is not obvious. In Tibet, most of the late Cenozoic potassic volcanism centers lie in the northern parts of the plateau, hundreds of kilometers from the locus of convergence in the Himalaya to the south [*Turner et al.*, 1996]. In the eastern Anatolian region of Turkey, the most potassic volcanism is found in the north (in the Erzurum-Kars Plateau region) since ≈11 Ma, several hundred kilometers from the site of subduction in the south where Eurasia and Arabia collided [*Keskin*, 2003; *Keskin et al.*, 1998; *Pearce et al.*, 1990]. In northeast China lower lithosphere is thought to have been removed beneath the middle of the otherwise undeformed North China Craton, with volcanism spiking around 120 Ma [*Gao et al.*, 2008].

[9] To evaluate the rheological conditions under which a Rayleigh-Taylor instability develops into this alternate style of downwelling with remote thinning of the unstable layer, we use two-dimensional plane-strain numerical calculations of the instability of a dense layer overlying a less dense half-space, subject to an initial harmonic perturbation on its lower boundary. We use a shear stress-free top boundary condition on the layer and examine spatially variable rheological properties. Calculations are carried out until the vertical displacement of the lower surface at least approaches initial layer thickness. If indeed the conditions for this type of instability occur on the Earth, it could indicate a mechanism for volcanism several hundred kilometers from active or previously active plate boundaries.

2. Basic Theory of Rayleigh-Taylor Instability and Small Slope Approximation

[10] Linearized theory is a common approach used to examine the growth of Rayleigh-Taylor instabilities [e.g., *Conrad and Molnar*, 1997; *Chandrasekhar*, 1961]. The approximations used must, of course, eventually fail as perturbations grow to large amplitudes and nonlinear terms in the governing equations become large, but the methods capture the initial growth of the instability, provide simplicity to a complex process, and can guide the development of scaling relationships. *Canright and Morris* [1993] developed small slope solutions for the growth of instabilities in a layer with constant rheological properties bounded by shear stress-free surfaces on the top and bottom of the unstable layer. Using an approach that explicitly includes the nonlinear interactions, they were able to describe unstable behavior at amplitudes larger than is possible with the linear approximation. They show the narrowing of deformation zones, and hence the separation of downwelling and upwelling, with increasing stress-strain exponent, n (see

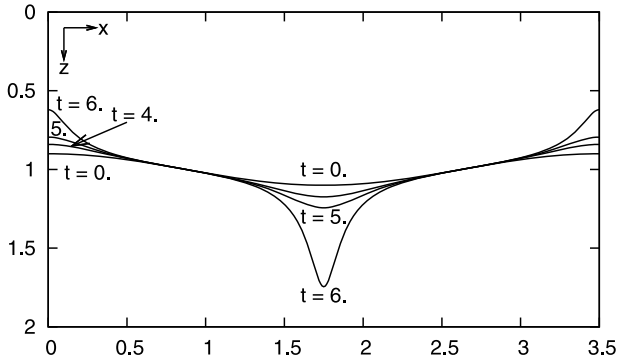

Figure 1. Boundary deflection profiles calculated as in the work of *Canright and Morris* [1993, Appendix B]. Here a constant density fluid of thickness 1, with power-law exponent of $n = 3$ is perturbed sinusoidally with amplitude 0.1. Dimensionless times $t = 0$, 4, 5, 6 shown. The solution derived by *Canright and Morris* [1993] is independent of the perturbation wavelength.

appendix in the work of *Canright and Morris* [1993]). We investigate this behavior further with numerical experiments, but we first examine the limits of the small slope theory.

[11] *Canright and Morris* [1993] examined three types of initial conditions, but the most appropriate for comparison with our experiments is a constant wavelength sinusoidal perturbation (wavelength λ) to the thickness of the unstable layer. Their solution for the change in layer thickness (δ) with time (t) for non-Newtonian viscosity obeys the following equation:

$$\frac{D\delta}{Dt} = sgn(\delta - d_e(t))\delta\left[\frac{|\delta^2 - d_e^2(t)|}{\delta}\right]^n \tag{1}$$

with

$$d_e^2(t) = \frac{\int_0^\lambda \delta\, dx}{\int_0^\lambda 1/\delta\, dx} \quad \text{and} \quad \frac{D\delta}{Dt} = \frac{\partial\delta}{\partial t} + u\frac{\partial\delta}{\partial x} \tag{2}$$

where δ is the thickness of the unstable layer and u is the horizontal component of velocity. When we consider the maximum and minimum thickness of the layer, u is zero, so at these positions $D\delta/Dt$ is just the change of thickness with time. *Canright and Morris* [1993] nondimensionalize quantities by the time scale $(\frac{4B}{\Delta\rho g h})^n$ and length scale by h, the initial thickness of the unstable layer. Here, $\Delta\rho$ is the density difference between the layer and lower half-space, and g is gravitational acceleration. B, the viscosity coefficient of the layer (when constant), and n, the rheological exponent are part of the nonlinear constitutive relation between deviatoric stress, τ_{ij}, and strain rate, $\dot{\epsilon}_{ij}$, defined in our layer:

$$\tau_{ij} = B_o exp(z/L)\dot{E}^{(1/n-1)}\dot{\epsilon}_{ij}. \tag{3}$$

This form includes an exponential depth-dependence of viscosity that we use later, with B_o as the viscosity coefficient at the lower surface, z as the vertical coordinate, set to zero at the bottom of the layer and increasing upward, and L as the e-folding depth scale for the exponential decrease (the depth interval across which the viscosity changes by a factor of e). Our analysis below depends on the dimensionless viscosity stratification ratio, h/L, which can be easily calculated for an olivine rheology [*Conrad and Molnar*, 1997]. Estimates of this ratio for conditions in the Sierra Nevada vary between 5 and 9 [*Harig et al.*, 2008]. $\ddot{E} = \sqrt{\sum_{i,j}\dot{\epsilon}_{ij}\dot{\epsilon}_{ij}}$ is the second invariant of the strain-rate tensor. This definition follows the convention of *Houseman and Molnar* [1997] and affects the definition of B values.

[12] We present results in an alternative nondimensionalization, defined by the time scale $(\frac{B_o}{\Delta\rho g h})^n$ from Figure 2 onward to conform to earlier work [e.g., Molnar et al. 1998]. *Canright and Morris* [1993] calculated boundary deformation through time (Figure 1), ensuring volume is conserved

$$\int_0^\lambda \left[\frac{\delta^2 - d_e^2(t)}{\delta}\right]^n dx = 0. \tag{4}$$

[13] We first validate the approximate theory by using the boundary deformation from our numerical experiments to calculate, using equation (1), $D\delta/Dt$ where the downwelling is maximum at different stages of growth. When we compare these rates to the numerically calculated downward component of dimensionless velocity, w' (Figure 2), we notice that the rate of downwelling predicted by the analytical approximation is systematically greater than that produced by the numerical calculation and the difference

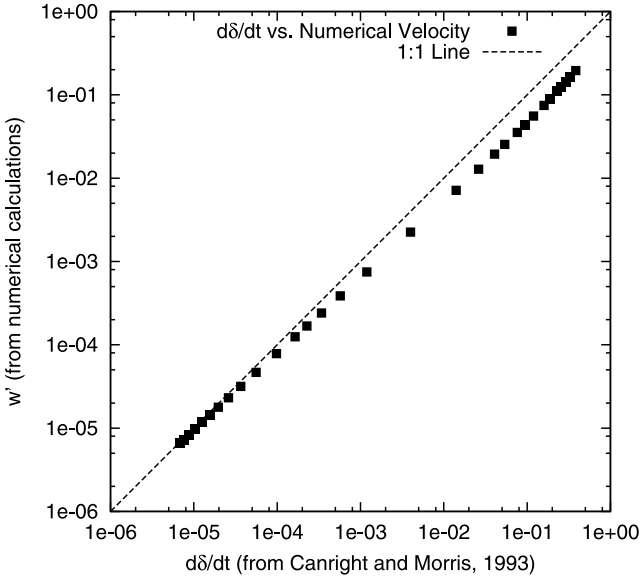

Figure 2. Value of log[Dδ/Dt] from equation (1) with δ obtained from finite element solution versus log[downward component of velocity] from numerical calculations. A 1:1 line is also shown. Cases here use $\lambda/h = 4\pi$.

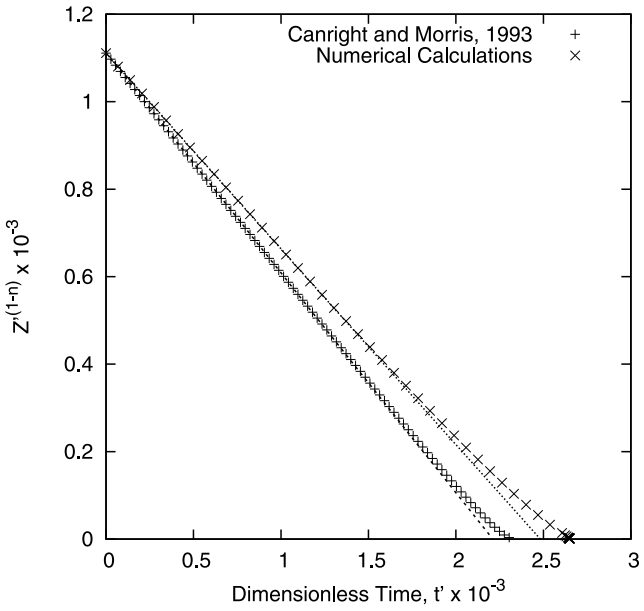

Figure 3. $Z'^{(1-n)}$ versus dimensionless time for the example where $n = 3$. Lines of the form in equation (5) are fit to the initial small-amplitude deformation portion of the data. The numerical case here uses $\lambda/h = 4\pi$.

increases as the instability grows. Alternatively, we can compare the peak deflection versus time for the two methods by numerical integration of $D\delta/Dt$. Following *Houseman and Molnar* [1997], we compare the growth rates by fitting lines of the form

$$Z'^{(1-n)} = (n-1)\left(\frac{C}{n}\right)^{n}(t'_b - t') \tag{5}$$

where the singular time t'_b represents the time when the downwelling reaches infinite depth (Figure 3). This form is derived from simple assumptions including an approximation to the nonlinear constitutive relation and that the stresses driving the instability are proportional to its interface deflection [*Houseman and Molnar*, 1997]. Here we see that the line fitting $Z'^{(1-n)}$ versus t' will give C from the slope and t'_b from the time intercept. The small slope approximation and numerical calculation appear to show initial agreement, but with different growth rates C, and correspondingly different estimates of the singular time t'_b.

[14] Inherent in Canright and Morris's derivation is the assumption of small slopes of the boundaries. While the slopes remain small, the layer has a large horizontal length scale compared to its vertical thickness. Away from the ends, horizontal components of velocity dwarf vertical components, and it is assumed these components of velocity are independent of the vertical coordinate. Their analysis ignores shear stress on horizontal planes, τ_{xz}. These assumptions start to fail as amplitudes of deformation become large (in this example, on the order of 10% thickness change), and this failure is likely the main reason for the small divergence between our numerical calculations and their approximate theory. In detail Canright and Morris's analysis is imperfect, but it provides a sensible qualitative image of the process and guides our work below.

3. Depth Varying Rheological Properties

3.1. Constant Density

[15] To complement the small amplitude analysis, we perform two-dimensional plane strain numerical Rayleigh-Taylor instability experiments with depth varying viscosity and categorize the instabilities according to the observed end states. Like *Houseman and Molnar* [1997], we use the finite element program Basil and begin with layers of constant density. We vary the depth-dependence of viscosity and the rheological exponent of the layer. Layer thicknesses are perturbed with a dimensionless wavelength of $\lambda' = \lambda/h = 4\pi$, with amplitude $0.03h$ or $0.04h$, chosen because there is qualitatively little difference in results once wavelength is sufficiently long ($\lambda' > 2\pi$). Our calculations do not include the energy equation, but previous experiments on convective instability including diffusion of heat [*Conrad and Molnar*, 1999], confirm the scaling laws of *Houseman and Molnar* [1997].

[16] Holding wavelength constant, instabilities fall within 3 groupings based mainly on the ratio of layer thickness to viscosity length scale, h/L (Figure 4). When $h/L \leq 2$, instabilities develop with zones of downwelling and upwelling separated by a broad region where vertical components of velocity are negligible. Within this central region horizontal velocity, U_x, is nearly constant in both x and z directions throughout the run. The entire central region moves as a coherent block toward the downwelling region. Also, as the calculation time nears t_b, maximum vertical deflection and velocity of the downwelling and upwelling are of comparable magnitude.

[17] When $h/L \geq 4$, the large viscosity contrast between the top and bottom of the layer enables deformation to concentrate near the bottom part of the layer and the horizontal component of velocity near the top is minimized. Thus significant vertical gradients of horizontal velocity now exist within the central region, and shear strain occurs on horizontal planes in the lower part of the layer. It should be clear that in this case the approximation of negligible shear stress on these planes, made by *Canright and Morris* [1993] for a layer with constant viscosity, is no longer valid. Furthermore the rates of vertical displacement differ greatly for thickening (downwelling) and thinning (upwelling); these rates differ at short times into the calculation and by increasing amounts as the duration of the calculation approaches the time t'_b. As h/L increases we see that the maximum thinning factor achieved is decreased as extension is distributed over a broader area of the lower lithosphere.

[18] The impact of h/L on vertical gradients of horizontal velocity is easily seen in the examples shown in Figure 4. The end member groupings show significantly different shear strain rate fields, which are indicative of their different later deformation patterns. For the calculation with $h/L = 4$, denoted with an X, we see the shear strain rate field contains vertically stratified positive values, indicating the field is dominated by $\partial u/\partial z$ as the lower part of the layer moves toward the downwelling. Conversely, the case with $h/L = 0.5$ (solid circle) has two separated areas of positive values

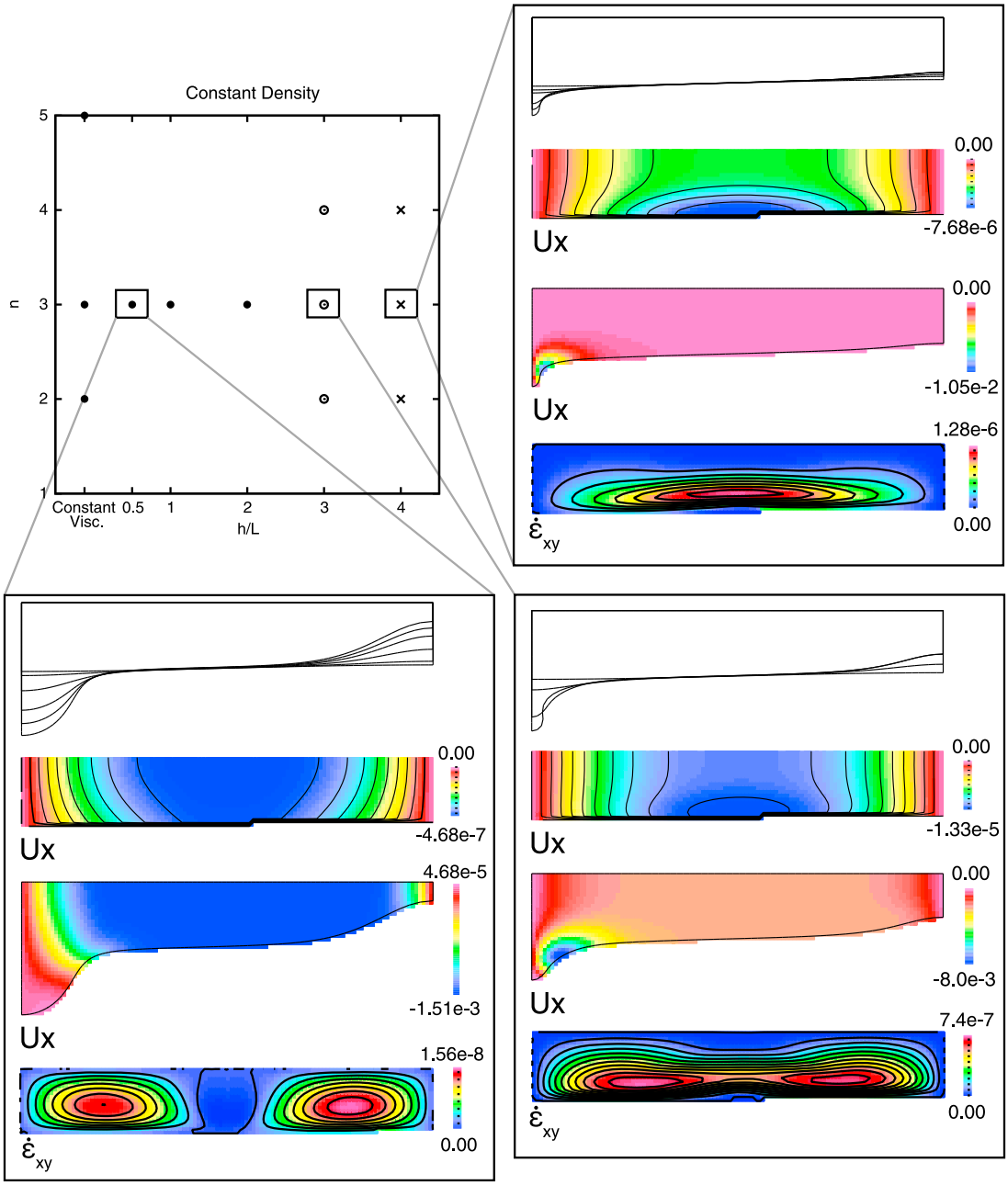

Figure 4. Phase diagram for experiments with constant density showing the division of instabilities based on their end state deformation. Instabilities divide into categories depending on viscosity stratification ratio h/L and stress-strain exponent n. In each case, $\lambda/h = 4\pi$. Closed circles are calculations in which center region develops uniform horizontal velocity. Crosses are calculations that develop significant shear deformation in the lower part of the layer and more distributed thinning. Open circles are transitional cases. One calculation from each group has additional detail showing different aspects of deformation. The first (top) detail shows boundary deformation through time while the second and third details are colored contours of horizontal velocity at the initial and later states. Negative values of horizontal velocity show motion to the left, toward the downwelling. Finally, $\dot{\epsilon}_{xy}$ is shown, indicating whether the dominant initial deformation is horizontal shear near the base of the layer or vertical shear at the ends of the calculation.

at the ends of the calculation. Here, $\partial u/\partial z$ is modest and the shear strain rate maxima are likely a result of positive values of $\partial w/\partial x$ corresponding to the downwelling at one end and the upwelling at the other. These two end member groups merge in a transition region (Figure 4, open circle) where one sees both concentrations of shear strain rate at the ends of the layer and a vertical gradient of strain rate in the center region.

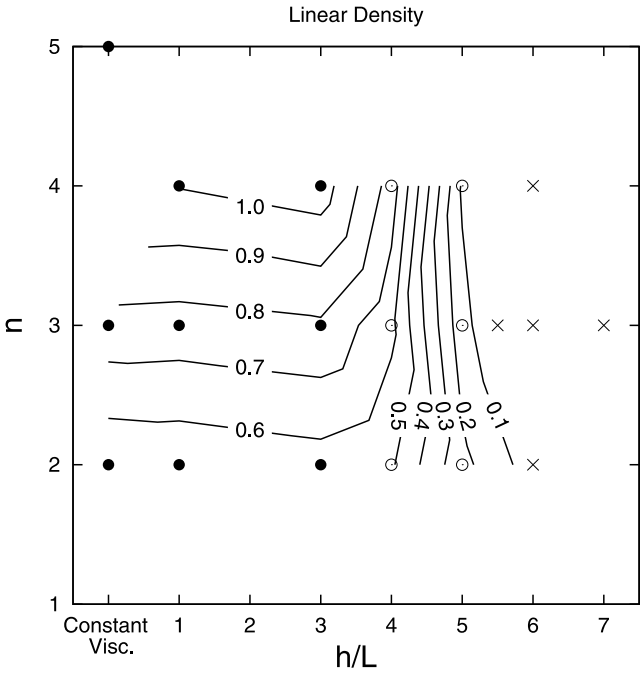

Figure 5. Phase diagram for experiments with linearly varying density ($\lambda/h = 4\pi$) showing the division of instabilities into categories depending on viscosity scaling h/L and stress-strain exponent n. Symbols are the same as Figure 4. Here we also plot contours of the absolute value of the ratio of upwelling speed to downwelling speed for the time when the downwelling zone has thickened by 40% (to 140% of original thickness).

3.2. Linearly Varying Density With Depth

[19] We also perform experiments with density varying linearly as a function of depth from zero at the base of the layer to two at the top. As before, instabilities grow into different end states depending mainly on the viscosity stratification ratio, h/L (Figure 5). The most noticeable difference for linearly varying density is the shift of the transition region from $2 < h/L < 4$ in constant density to $3 < h/L < 6$ with linearly decreasing density anomaly. Of course, this assessment of the width of the transition zone, based on the horizontal speed, is subjective. As a more objective measure we calculate the absolute value of the ratio of maximum upwelling speed to maximum downwelling speed at a time when the downwelling zone has thickened by 40% (or is 140% of original thickness). The contours in Figure 5 allow a more precise definition of the transition zone limited by vertical contours at large h/L and horizontal contours at small h/L. The contours also roughly indicate the maximum thinning we should expect; ratios near one indicate the layer approaches the upper limit of thinning to zero thickness.

[20] We note that h/L and n have different effects on the final deformation of the layer, with the rheological exponent controlling the final large amplitude superexponential growth. If two cases have similar velocity ratios, a lower n means the final stages of drip formation will be less abrupt and the layer can continue to thin. Alternatively, when a case with large n reaches t_b the downwelling will develop much faster than further thinning.

[21] For example cases with $n = 2$, and $h/L = 6$ or 3 we examine the growth of the upwelling and downwelling (Figure 6) to see where they diverge. When the upwelling is localized (Figure 6a), the maximum upwelling and downwelling deflections are well approximated with the $Z'^{(1-n)}$ fits even as they approach the singular time t'_b. When thinning is distributed over a wider region (Figure 6b) the

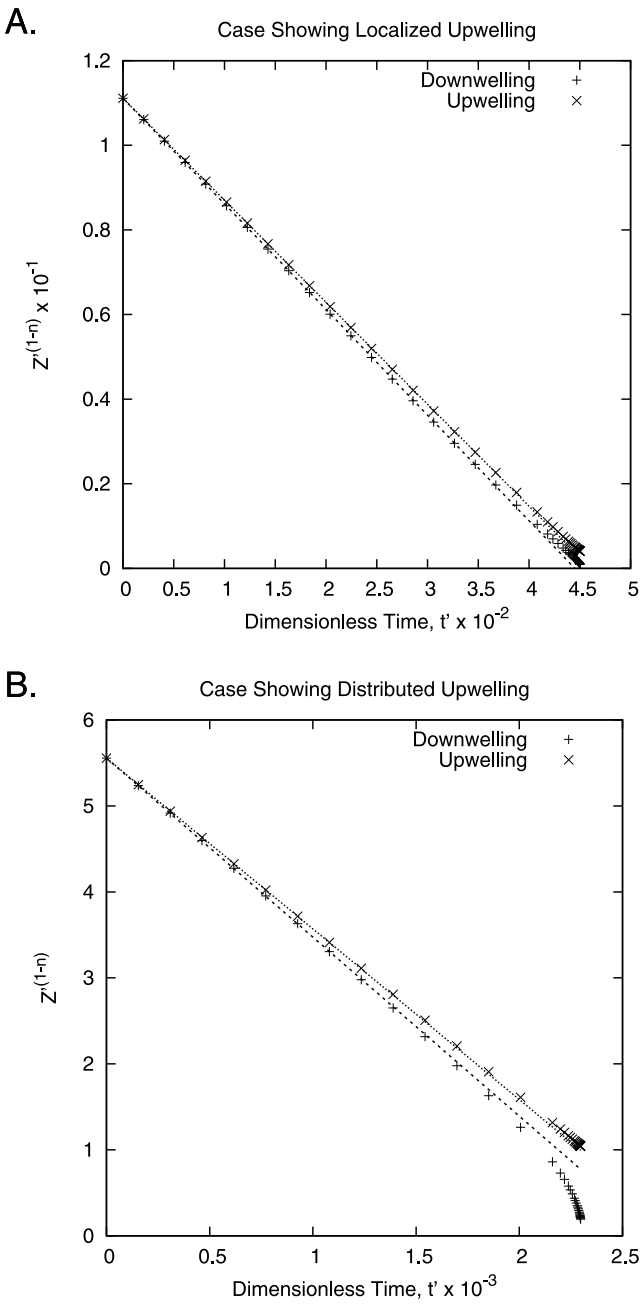

Figure 6. $Z'^{(1-n)}$ versus t' for both upwellings and downwellings for cases with $\lambda/h = 4\pi$, $n = 2$, and density decreasing linearly with depth, showing (a) a case with localized upwelling with $h/L = 3$ and (b) a case with $h/L = 6$ and distributed upwelling. Best fit lines are drawn from equation (5).

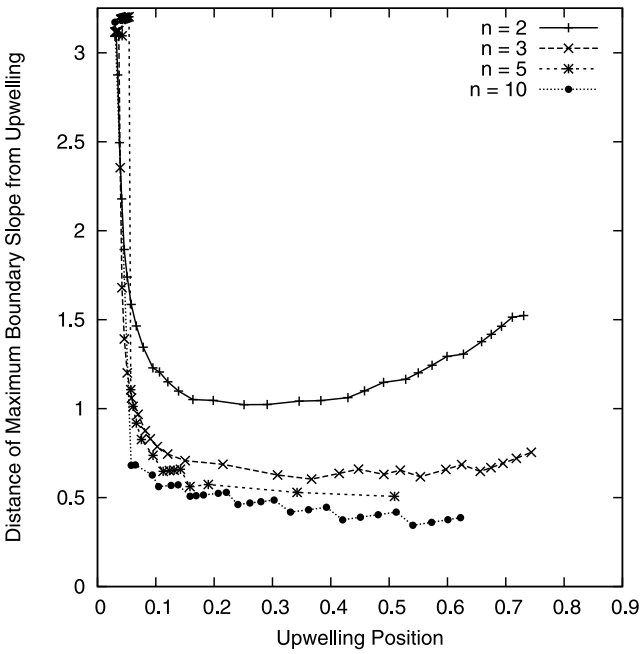

Figure 7. A comparison of the horizontal position of the local maximum in lower boundary slope for the upwelling plotted against maximum vertical upwelling position, as each instability develops. Vertical position can be considered a proxy of the timescale across experiments because the vertical position increases monotonically with each calculation step. Each case has constant viscosity coefficient and constant density in the layer, with $\lambda/h = 4\pi$. The local maximum in lower boundary slope initially begins at π due to the imposed perturbation and quickly becomes more localized at the upwelling zone.

downwelling deflection deviates from its best fit and approaches the time t'_b much sooner than estimated from the fit. The upwelling deflection, however, continues to follow the power law growth trend established early in the calculation.

3.3. Variation With Stress Exponent, *n*, and Viscosity Scaling, *h*/*L*

[22] To evaluate the effects of different exponents in the constitutive relationship, n, we examine cases with constant viscosity coefficient ($L \rightarrow \infty$) for which separated upwellings and downwellings occur. Although initially perturbed with a harmonic variation in the thickness of the unstable layer, these cases quickly transition to localized thinning and downwellings. As *Canright and Morris* [1993] found, once λ' is large enough, the form of deformation should vary with wavelength only as a simple scaling (or stretching). The cases examined here were perturbed with $\lambda' = 4\pi$, which should be considered for dimensionalization. To quantify the transition to localized deformation we examine the half-width of the upwelling zone, which we define as the position of the local maximum of the slope of the base of the layer (Figure 7). These positions are calculated for each time step using the first-order finite difference between the lower surface nodes but are plotted versus vertical displacement at the center of the upwelling (as opposed to versus time) since each experiment uses a different timescale. With increasing n, the width of the upwelling zone decreases, further localizing deformation, as predicted by *Canright and Morris* [1993]. The steps in the horizontal positions in Figure 7 can be attributed, we believe, to times when maximum slope moves from one boundary node to another.

[23] *England et al.* [1985] examined the length scales of continental deformation for different plate boundary settings. With some simplification, they solved for the velocity field in a thin viscous sheet perpendicular to a convergent or divergent margin. They found that this component of velocity decreases with distance from the margin as $e^{-\sqrt{n}\pi y/\lambda}$. In this case, λ was the wavelength of their boundary perturbation. Our two-dimensional calculation, with a center region that moves uniformly away from the upwelling boundary, is similar in setting to the convergent/divergent boundary considered by *England et al.* [1985]. The main difference here is that the velocity parallel to the vertical symmetry plane is not zero.

[24] We estimate where each upwelling width stabilizes in Figure 7, noting the variability or uncertainty in our estimate, and plot them versus rheological exponent in Figure 8. The width of the upwelling zone roughly follows the relation

$$\text{width} \approx 1.25 n^{-1/2}, \tag{6}$$

scaled by the perturbation wavelength.

[25] We also examine the velocity profile, u, along the top shear stress free surface at the initial time step. We find that,

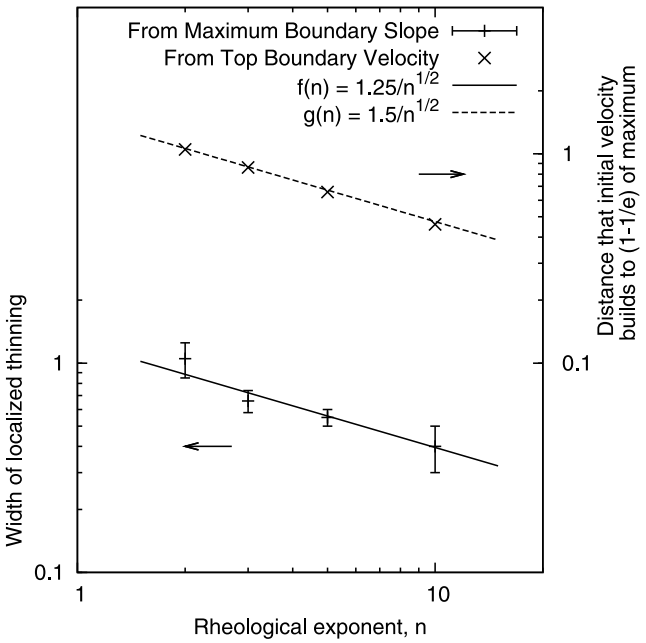

Figure 8. Estimates of the width of the localized upwelling region versus rheological exponent n, estimated from the maximum slope of the bottom boundary (lower line, left-hand scale). Widths and uncertainties are estimated from Figure 7. In the upper part of the graph we plot the distance over which horizontal velocity on the top boundary decays away from the symmetry plane versus rheological exponent n. These data use the right-hand y axis.

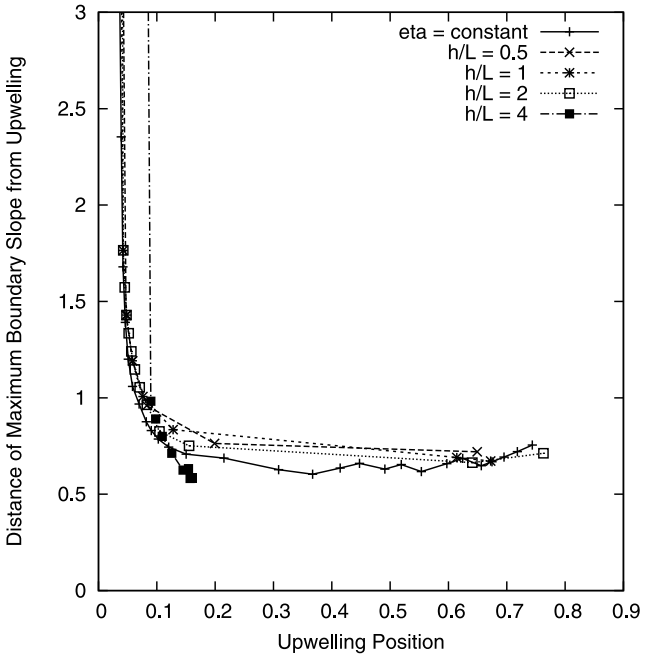

Figure 9. We plot, as in Figure 7, the upwelling zone width versus upwelling deformation for cases with $n = 3$. Each case has constant viscosity coefficient and constant density in the layer, with $\lambda/h = 4\pi$. Those cases that develop with separated upwellings and downwellings, $h/L < 4$, show little variation with length scale of viscosity variation. The case of $h/L = 4$ does not develop with separated upwellings and downwellings, and upwelling deformation remains minimal compared to downwelling deformation (54% of layer thickness in this case).

although it is not a simple exponential function, the distance required for the maximum horizontal velocity to build to $(1 - 1/e)$ of the maximum very closely follows the relation $\approx 1.5 * n^{-1/2}$ (also Figure 8). It seems that although our calculations include greater complexity than those of *England et al.* [1985], the underlying dependence on the square root of the rheological exponent, n, still applies when the medium adequately approximates a half-space perpendicular to the symmetry plane (in our case when $\lambda > \pi$).

[26] Variation of the width of the upwelling with viscosity stratification ratio, h/L, is examined in Figure 9. Here the rheological exponent $n = 3$ for each case. The width of the upwelling region shows little dependence on h/L except when $h/L \geq 4$ (when broad distributed thinning occurs). Since we might expect h/L values for lower lithosphere to vary between 5 and 9, this shows that when the high-temperature stress strain exponent of $n = 3.5$ for olivine is used for the entire lithosphere, localized thinning would be unlikely.

4. Discussion

4.1. Large-Scale Lower Lithosphere Removal

[27] The zone of plate-like deformation occurs when $h/L < 3$ and is below the range of values we might expect in typical lower lithosphere, which can range from roughly 5 to 9 [*Harig et al.*, 2008]. The h/L ratio of the power law rheology of olivine is determined approximately as

$$\frac{h}{L} = \frac{E_a \Delta T}{n R T_0^2} \tag{7}$$

where E_a is activation energy which can vary between 430 and 540 kJ/mol [*Karato and Wu*, 1993], ΔT is the temperature variation across the layer, n is the stress strain constitutive exponent often fixed at 3.5 (based on creep measurements of dry olivine), R is the gas constant (8.314472 J K^{-1} mol^{-1}), and T_0 is the temperature at the base of the layer [*Harig et al.*, 2008]. With this rheology, $h/L < 3$ requires either unreasonably warm Moho ($T \approx 900°C$ for a mantle potential temperature of $T_0 = 1300°C$, $\Delta T = 400°C$) or a transition to the low-temperature high-stress creep regime which results in a greater effective value of n [*Evans and Goetze*, 1979; *Goetze*, 1978].

[28] At high stresses the power law constitutive equation for olivine breaks down to an exponential relation between stress difference and strain rate experimentally given by *Goetze* [1978] and *Evans and Goetze* [1979] as

$$\dot{\epsilon}_{11} = \dot{\epsilon}_0 exp\left[-\frac{H_a}{RT}\left(1 - \frac{\sigma_{11} - \sigma_{33}}{\sigma_0}\right)^2\right]. \tag{8}$$

Here $\dot{\epsilon}_{11}$ is the longitudinal strain in a uniaxial strain rate experiment, and $\sigma_{11} - \sigma_{33}$ is the difference between longitudinal compressive stress and confining pressure. *Molnar and Jones* [2004] rewrite this in the constitutive form of equation (3) as

$$\tau_{ij} = \frac{\dot{\epsilon}_{ij}}{\dot{E}\sqrt{3}}\sigma_0\left[1 - \left(\frac{RT}{H_a} ln \frac{\sqrt{3}\dot{\epsilon}_0}{2\dot{E}}\right)^{1/2}\right]. \tag{9}$$

The quantities $\dot{\epsilon}_0$, σ_0, and H_a are experimentally determined and given by *Goetze* [1978] to be $\epsilon_0 = 5.7 * 10^{11}$ s^{-1}, $\sigma_0 = 8.5$ GPa, and $H_a = 536$ kJ/mol, and other symbols are as in the notation section. In this form, *Molnar and Jones* [2004] compared the high-stress effective viscosity coefficient to that from the power law relation, equation (3). They determined that for geologically relevant strain rates, $10^{-13} - 10^{-15}$ s^{-1}, this high-stress law would apply in the upper portions of the mantle lithosphere where temperatures are below $\approx$800–1000°C [*Goetze*, 1978; *Molnar and Jones*, 2004; *Tsenn and Carter*, 1987]. This high-stress law may also be well approximated using a power law with $n \geq 10$ for which stresses are rather insensitive to strain rates [e.g., Dayem et al. 2009]. Using $n = 10$ in equation (7) means that h/L becomes about 3, whereas for $n = 3.5$ it is about 8. If n is effectively 10, as it would be if dominated by the low-temperature flow law, then upper portions of the mantle lithosphere have the potential to be dynamically removed by this mechanism, along with the lower portions of the layer.

[29] The assumption of a zero shear stress condition at the base of the crust represents one possible end member boundary condition and can be justified geologically in several ways. One could argue that the lower crust should be weak compared to the upper mantle when it is suffi-

ciently warm. Evidence of an eclogitic layer at the base of the crust could also suggest this boundary condition [e.g., *Harig et al.*, 2008] as eclogite is thought to deform at lower viscosities than granulite [e.g., *Austrheim*, 1991]. Finally, a quartz-rich crust also has the potential to flow at relatively low shear stress at typical Moho temperatures [e.g., *Brace and Kohlstedt*, 1980; *Sibson*, 1977, 1982]. Even at high pressures these flow stresses for quartz remain below a few MPa and microstructures suggest the stresses do not even reach this threshold to transition to dislocation creep [*Stöckhert and Renner*, 1998].

4.2. Intracontinental Magmatism

[30] With a shear stress-free upper boundary, rheological exponent $n \geq 2$, and $\lambda' \geq 6$ downwellings and upwellings are separated by a central region that has relatively low internal strain rate and near uniform horizontal velocity and that moves as almost a coherent block. This suggests that localized thinning could be offset several hundred kilometers from the zone of downwelling.

[31] Although potassic magmas can result from various triggers, they may link to lithospheric instabilities in several plate boundary regions. In the Sierra Nevada, broad high-potassium magmatism is one of several observations that indicate removal of lower lithosphere (in this case within 100 km of inferred downwelling). These volcanics of varying type [e.g., *Farmer et al.*, 2002] are inferred to have lithospheric mantle sources that have been metasomatized in a previous arc magmatism setting, as opposed to a depleted mantle source [e.g., *Turner et al.*, 1996]. The convective removal of lower lithosphere allowed the lithospheric mantle to melt where thinned, either adiabatically in upward flow [e.g., *Elkins-Tanton and Grove*, 2003] or by simple conductive heating of shallow lithosphere exposed to hot asthenosphere [e.g., *Farmer et al.*, 2002], causing an abrupt pulse of magmatism at ~3.5 Ma.

[32] Generally, since the metasomatism of lower lithosphere is preserved for as long as temperatures in the lithosphere remain below the solidus, these magmas are also possible away from current or geologically recent subduction zones, in settings that could have had subduction influences further back in time [*Elkins-Tanton*, 2005, 2007]. For instance, much of the western United States can be assumed to have been hydrated by low angle subduction in the early Cenozoic [*Farmer et al.*, 2008]. This potassic magmatism may also follow dry adiabatic melting of asthenosphere if the downwelling lithosphere releases hydrous volatiles as it sinks to greater pressures [*Elkins-Tanton*, 2005, 2007; *Elkins-Tanton and Hager*, 2000].

[33] Melting in the localized upwelling zone should be controlled by the deflection of the lithosphere-asthenosphere boundary (Figure 4), the width of which depends on the rheological exponent, n (Figure 8). This melting ought not occur throughout the entire column of mantle lithosphere. While material near the top of the column would move upward adiabatically, its initially low temperature would prevent it from reaching its solidus and hence melting.

[34] The localization of the upwelling zone when h/L is less than about three implies that when a shear stress-free surface might be applicable, magmatism could play an even more important role than considered previously. First, thinning, and hence magmatism, need not occur near plate boundaries, where large stresses and strains can easily create the perturbation necessary to induce gravitational instability. Magmatism instead may appear several hundred kilometers into the continental plate. There, increased lithospheric thicknesses may hide surface indicators of thinning or extension such as rapid change of surface elevations or rifting. Second, magmatism may be more diagnostically important at smaller horizontal length scales than can be resolved with other techniques such as travel time tomography or receiver function analysis. It may be that shorter-scale, unresolved lithospheric instabilities occur, requiring densely spaced seismic networks for detection [*Yang and Forsyth*, 2006]. In this case, the high-potassium magmatism may be the best evidence with which to begin an investigation of lithospheric removal induced by convective or Rayleigh-Taylor instability.

5. Conclusions

[35] When the dimensionless wavelength of the perturbation, λ' (ratio of perturbation wavelength to layer thickness), is greater than approximately six, and shear stress on the upper surface is negligible, a power law rheology causes two-dimensional Rayleigh-Taylor instability to separate into two forms, controlled by viscosity, density, and stress strain exponent. For low-viscosity stratification ratios, $h/L \leq 2$ (for constant density) or $h/L \leq 3$ (for depth-dependent density), deformation concentrates at the ends of the unstable layer as localized upwelling and downwelling. The middle part of the layer moves horizontally towards the downwelling as a coherent block. Throughout the growth of the instability, the upwelling and downwelling grow at comparable rates.

[36] As h/L increases, the similarities between upwelling and downwelling diverge. The vertical viscosity variation permits vertical gradients in horizontal velocity and prevents the middle area from ever moving as a coherent block. Upwelling deformation is distributed over a broader area of the lower lithosphere and total thinning remains small as downwelling peaks.

[37] The transition zone for intermediate values of h/L reflects a combination of these two end states. The initial growth of the instabilities mirrors those with separated upwellings and downwellings, which grow at similar rates, and a middle zone with subtle vertical gradients in horizontal velocity. Final stages of growth are similar to cases with large h/L, with downwelling growing rapidly and upwelling becoming more diffuse. This transition type appears at slightly higher viscosity stratification ratios with the introduction of depth varying density.

[38] The estimated width of the maximum upwelling zone is controlled by the rheological exponent in the constitutive equation and varies as $\approx n^{-1/2}$. The decay in horizontal velocity away from the side boundaries of our layer also indicates a $\approx n^{-1/2}$ relation. Together they compare well to earlier studies of deformation length scales for a half-space deformed by boundary stresses [*England et al.*, 1985].

[39] We suggest the low-viscosity stratification ratio required for plate-like deformation ($h/L < 3$) is plausible when considering the high-stress low-temperature creep regime. Approximating this regime with a $n > 10$ power law rheology can reduce the effective h/L to the $h/L < 3$

range. Without the high-stress regime, low h/L ratios are less realistic, and high values of B at low temperatures would prevent upper portions of the mantle lithosphere being removed when dynamical instability occurs. The Sierra Nevada, however, provides a counter example; estimates of the lithosphere's thermal structure prior to 10 Ma indicate removal of tens of kilometers of material colder than 900°C [e.g., *Molnar and Jones*, 2004] has occurred.

Notation

- B Viscosity coefficient (where constant in the layer).
- B_0 Viscosity coefficient at the base of the layer, through which it decreases with depth.
- d_e Equilibrium thickness of the unstable layer defined by *Canright and Morris* [1993] as the thickness that has no tendency to grow or shrink.
- $\ddot{\text{E}}$ Second invariant of the strain rate tensor.
- E_a Activation energy.
- g Gravitational acceleration.
- H_a Experimentally determined activation energy constant (535 kJ/mol) in the high stress constitutive equation.
- h Initial thickness of layer.
- L Characteristic e-folding depth scale for exponential decrease in viscosity coefficient.
- n Rheological exponent in the stress-strain constitutive equation.
- p Pressure.
- R Gas-law constant.
- t Time.
- t_b Time when downwelling detaches from upper surface.
- T Temperature.
- T_0 Temperature at base of layer.
- ΔT Temperature difference across layer.
- u Horizontal component of velocity.
- w Vertical component of velocity.
- x Horizontal coordinate.
- z Vertical coordinate set to zero at the bottom interface of the layer and positive upward in our numerical cases.
- δ Thickness of layer as function of time, from *Canright and Morris* [1993].
- λ Wavelength of perturbation to layer.
- ρ Density.
- $\Delta\rho$ Density difference between the layer and the underlying half-space or subspace.
- ϵ_{ij} Strain component.
- $\dot{\epsilon}_{ij}$ Strain rate component.
- $\dot{\epsilon}_0$ Experimentally determined strain rate constant ($5.7 * 10^{11}$ s^{-1}) in the high stress constitutive equation.
- σ_{ij} Stress component.
- σ_0 Experimentally determined stress constant (8.5 GPa) in the high stress constitutive equation.
- τ_{ij} Deviatoric stress component.

[40] **Acknowledgments.** This research was supported by the National Science Foundation grant EAR-0607831, a CIRES Graduate Student Research Fellowship to C. Harig, and a W. O. Thompson Fund grant to C. Harig from the Department of Geological Sciences. We thank G. L. Farmer for helpful discussions and thank L. T. Elkins-Tanton and an anonymous reviewer for thoughtful and constructive reviews. Figures created with the GMT software [*Wessel and Smith*, 1998] and the open source software gnuplot.

References

Austrheim, H. (1991), Eclogite formation and dynamics of crustal roots under continental collision zones, *Terra Nova*, *3*, 492–499.

Brace, W. F., and D. L. Kohlstedt (1980), Limits on lithospheric stress imposed by laboratory experiments, *J. Geophys. Res.*, *85*, 6248–6252.

Canright, D., and S. Morris (1993), Buoyant instability of a viscous film over a passive fluid, *J. Fluid Mech.*, *255*, 349–372.

Chandrasekhar, S. (1961), *Hydrodynamic and Hydromagnetic Stability*, Oxford Univ. Press, Oxford, U. K.

Conrad, C. P., and P. Molnar (1997), The growth of Rayleigh-Taylor-type instabilities in the lithosphere for various rheological and density structures, *Geophys. J. Int.*, *129*, 95–112.

Conrad, C. P., and P. Molnar (1999), Convective instability of a boundary layer with temperature and strain-rate-dependent viscosity in terms of 'available buoyancy', *Geophys. J. Int.*, *139*, 51–68.

Dayem, K. E., G. A. Houseman, and P. Molnar (2009), Localization of shear along a lithospheric strength discontinuity: Application of a continuous deformation model to the boundary between Tibet and the Tarim Basin, *Tectonics*, *28*, TC3002, doi:10.1029/2008TC002264.

Ducea, M. N., and J. B. Saleeby (1996), Bouyancy sources for a large, unrooted mountain range, the Sierra Nevada, California: Evidence from xenolith thermobarometry, *J. Geophys. Res.*, *101*(B4), 8229–8244.

Elkins-Tanton, L. T. (2005), Continental magmatism caused by lithospheric delamination, *Spec. Pap. Geol. Soc. Am.*, *388*, 449–461.

Elkins-Tanton, L. T. (2007), Continental magmatism, volatile recycling, and a heterogeneous mantle caused by lithospheric gravitational instabilities, *J. Geophys. Res.*, *112*, B03405, doi:10.1029/2005JB004072.

Elkins-Tanton, L. T., and T. L. Grove (2003), Evidence for deep melting of hydrous metasomatized mantle: Pliocene high-potassium magmas from the Sierra Nevadas, *J. Geophys. Res.*, *108*(B7), 2350, doi:10.1029/2002JB002168.

Elkins-Tanton, L. T., and B. H. Hager (2000), Melt intrusion as a trigger for lithospheric foundering and the eruption of the Siberian flood basalt, *Geophys. Res. Lett.*, *27*, 3937–3940.

England, P., G. Houseman, and L. Sonder (1985), Length scales for continental deformation in convergent, divergent, and strike-slip environments: Analytical and approximate solutions for a thin viscous sheet model, *J. Geophys. Res.*, *90*, 3551–3557.

Evans, B., and C. Goetze (1979), Temperature variation of hardness of olivine and its implication for polycrystalline yield stress, *J. Geophys. Res.*, *84*, 5505–5524.

Farmer, G. L., A. F. Glazner, and C. R. Manley (2002), Did lithospheric delamination trigger late Cenozoic potassic volcanism in the southern Sierra Nevada, California?, *Geol Soc. Am. Bull.*, *114*, 754–768.

Farmer, G. L., T. Bailley, and L. T. Elkins-Tanton (2008), Mantle source volumes and the origin of the mid-Tertiary ignimbrite flare-up in the southern Rocky Mountains, western U.S., *Lithos*, *102*, 279–294.

Gao, S., et al. (2008), Recycling deep cratonic lithosphere and generation of intraplate magmatism in the North China Craton, *Earth Planet. Sci. Lett.*, *270*, 41–53.

Gemmer, L., and G. A. Houseman (2007), Convergence and extension driven by lithospheric gravitational instability: Evolution of the Alpine-Carpathian-Pannonion system, *Geophys. J. Int.*, *168*, 1276–1290.

Goetze, C. (1978), Mechanisms of creep in olivine, *Philos. Trans. R. Soc. London*, *288*, 99–119.

Harig, C., P. Molnar, and G. A. Houseman (2008), Rayleigh-Taylor instability under a shear stress free top boundary condition and its relevance to removal of mantle lithosphere from beneath the sierra nevada, *Tectonics*, *27*, TC6019, doi:10.1029/2007TC002241.

Hoernle, K., J. D. L. White, P. van der Bogaard, F. Hauff, D. S. Coombs, R. Werner, C. Timm, D. Garbe-Schonberg, A. Reay, and A. F. Cooper (2006), Cenozoic intraplate volcanism on New Zealand: Upwelling induced by lithospheric removal, *Earth Planet. Sci. Lett.*, *248*, 335–352.

Hoogenboom, T., and G. A. Houseman (2006), Rayleigh-Taylor instability as a mechanism for corona formation on Venus, *Icarus*, *180*, 292–307.

Houseman, G. A., and P. Molnar (1997), Gravitational (Rayleigh-Taylor) instability of a layer with non-linear viscosity and convective thinning of continental lithosphere, *Geophys. J. Int.*, *128*, 125–150.

Jones, C. H., H. Kanamori, and S. W. Roecker (1994), Missing roots and mantle 'drips': Regional P_n and teleseismic arrival times in the southern Sierra Nevada and vicinity, California, *J. Geophys. Res.*, *99*(B3), 4567–4601.

Jones, C. H., G. L. Farmer, and J. Unruh (2004), Tectonics of Pliocene removal of the lithosphere of the Sierra Nevada, California, *Geol. Soc. Am. Bull.*, *116*(11/12), 1408–1422.

Jull, M., and P. B. Keleman (2001), On the conditions for lower crustal convective instability, *J. Geophys. Res.*, *106*(B4), 6423–6446.

Karato, S.-i., and P. Wu (1993), Rheology of the upper mantle: A synthesis, *Science*, *260*, 771–778.

Kay, R. W. (1980), Volcanic arc magmas: Implications of a melting-mixing model for element recycling in the crust-upper mantle system, *J. Geol.*, *88*, 497–522.

Kay, R. W., and S. M. Kay (1993), Delamination and delamination magmatism, *Tectonophysics*, *219*, 177–189.

Keskin, M. (2003), Magma generation by slab steepening and breakoff beneath a subduction-accretion complex: An alternative model for collision-related volcanism in Eastern Anatolia, Turkey, *Geophys. Res. Lett.*, *30*(24), 8046, doi:10.1029/2003GL018019.

Keskin, M., J. A. Pearce, and J. G. Mitchell (1998), Volcano-stratigraphy and geochemistry of collision-related volcanism on the Erzurum-Kars Plateau, North Eastern Turkey, *J. Volcanol. Geotherm. Res.*, *85*, 355–404.

Knapp, J. H., C. C. Knapp, V. Raileanu, L. Matenco, V. Mocanu, and C. Dinu (2005), Crustal constraints on the origin of mantle seismicity in the Vrancea Zone, Romania: The case for active continental lithospheric delamination, *Tectonophysics*, *410*, 311–323.

Lee, C.-T., R. L. Rudnick, and G. H. Brimhall Jr. (2001), Deep lithospheric dynamics beneath the Sierra Nevada during the Mesozoic and Cenozoic as inferred from xenolith petrology, *Geochem. Geophys. Geosyst.*, *2*(12), 1053, doi:10.1029/2001GC000152.

Lorinczi, P., and G. A. Houseman (2009), Lithospheric gravitational instability beneath the southeast Carpathians, *Tectonophysics*, *474*, 322–336.

Manley, C. R., A. F. Glazner, and G. L. Farmer (2000), Timing of volcanism in the sierra nevada of california: Evidence for pliocene delamination of the batholithic root?, *Geology*, *28*(9), 811–814.

McKenzie, D., and M. J. Bickle (1988), The volume and composition of melt generated by extension of the lithosphere, *J. Petrol.*, *29*(3), 625–679.

Molnar, P., and G. A. Houseman (2004), The effects of buoyant crust on the gravitational instability of thickened mantle lithosphere at zones of intracontinental convergence, *Geophys. J. Int.*, *158*, 1134–1150.

Molnar, P., and C. H. Jones (2004), A test of laboratory based rheological parameters of olivine from an analysis of late Cenozoic convective removal of mantle lithosphere beneath the Sierra Nevada, California, USA, *Geophys. J. Int.*, *156*, 555–564.

Molnar, P., G. A. Houseman, and C. P. Conrad (1998), Rayleigh-Taylor instability and convective thinning of mechanically thickened lithosphere: effects of non-linear viscosity decreasing exponentially with depth and of horizontal shortening of the layer, *Geophys. J. Int.*, *133*, 568–584.

Morris, J. D., W. P. Leeman, and F. Tera (1990), The subducted component in island arc lavas: constraints from Be isotopes and B-Be systematics, *Nature*, *344*, 31–36.

Pearce, J. A., J. F. Bender, S. E. De Long, W. S. F. Kidd, P. J. Low, Y. Güner, F. Saroglu, Y. Yilmaz, S. Moorbath, and J. G. Mitchell (1990), Genesis of collision volcanism in Eastern Anatolia, Turkey, *J. Volcanol. Geotherm. Res.*, *44*, 189–229.

Reeg, H., C. H. Jones, H. Gilbert, T. Owens, and G. Zandt (2007), Teleseismic travel-time tomography of the Sierra Nevada and its foundering lithosphere, *Eos Trans. AGU*, *88*(52), Fall Meet. Suppl., Abstract T33A-1150.

Sibson, R. H. (1977), Fault rocks and fault mechanisms, *J. Geol. Soc. London*, *133*, 191–213.

Sibson, R. H. (1982), Fault zone models, heat flow, and the depth distribution of earthquakes in the continental crust of the United States, *Bull. Seismol. Soc. Am.*, *72*, 151–163.

Stern, T., P. Molnar, D. Okaya, and D. Eberhart-Phillips (2000), Teleseismic P wave delays and modes of shortening the mantle lithosphere beneath South Island, New Zealand, *J. Geophys. Res.*, *105*(B9), 21,615–21,631.

Stern, T. A., W. R. Stratford, and M. L. Salmon (2006), Subduction evolution and mantle dynamics at a continental margin: Central North Island, New Zealand, *Rev. Geophys.*, *44*, RG4002, doi:10.1029/2005RG000171.

Stock, G. M., R. S. Anderson, and R. C. Finkel (2004), Pace of landscape evolution in the Sierra Nevada, California, revealed by cosmogenic dating of cave sediments, *Geology*, *32*, 193–196.

Stöckhert, B., and J. Renner (1998), Rheology of crustal rocks at ultrahigh pressure, in *When Continents Collide: Geodynamics and Geochemistry of Ultrahigh-Pressure Rocks*, edited by B. R. Hacker and J. G. Liou, chap. 3, pp. 57–95, Kluwer Acad., Dordrecht, Netherlands.

Tsenn, M. C., and N. L. Carter (1987), Upper limits of power law creep of rocks, *Tectonophysics*, *136*, 1–26.

Turner, S., N. Arnaud, J. Liu, N. Rogers, C. Hawkesworth, N. Harris, S. Kelley, P. V. Calsteren, and W. Deng (1996), Post-collision, shoshonitic volcanism on the Tibetan Plateau: Implications for convective thinning of the lithosphere and the source of ocean island basalts, *J. Petrol.*, *37*, 45–71.

Unruh, J. R. (1991), The uplift of the Sierra Nevada and implications for late Cenozoic epeirogeny in the western Cordillera, *Geol. Soc. Am. Bull.*, *103*, 1395–1404.

Wessel, P., and W. H. F. Smith (1998), New, improved version of generic mapping tools released, *Eos Trans. AGU*, *79*(47), 579.

Yang, Y., and D. W. Forsyth (2006), Rayleigh wave phase velocities, small-scale convection, and azimuthal anisotropy beneath southern California, *J. Geophys. Res.*, *111*, B07306, doi:10.1029/2005JB004180.

C. Harig and P. Molnar, Department of Geological Sciences, Cooperative Institute for Research in Environmental Science, University of Colorado at Boulder, Benson Earth Sciences Building, Boulder, CO 80309, USA. (harig@colorado.edu; molnar@colorado.edu)

G. A. Houseman, Institute of Geophysics and Tectonics, School of Earth and Environment, University of Leeds, Leeds LS2 9JT, UK. (greg@earth.leeds.ac.uk)